An adaptive electrodynamic metamaterial for the absorption of structural vibration

Lawrence Singleton, Jordan Cheer

[a] *Institute of Sound and Vibration Research, University of Southampton, University Road, Southampton, SO17 1BJ, Hampshire, UK*

Abstract

This paper presents an adaptive shunted electrodynamic metamaterial, for broadband robust vibration control. The study considers a unit cell of 12 miniature, low-cost proof-mass actuators for the control of vibration in a three degree-of-freedom structure subject to parametric uncertainty. In order to modify their dynamic responses, each actuator is connected to a shunt circuit consisting of a parallel resistor and a switched in/out inductor and capacitor. Provided the impedance of the actuator is cancelled out using a negative impedance, the shunt circuit is capable of tuning the resonance of the actuator up or down in frequency. An adaptive tuning approach is proposed, whereby the shunted actuator resonance frequencies are periodically switched to the centre frequencies of the highest magnitude bins of a real-time frequency analysis of the velocity measured on the structure. This approach is compared to a blind swept tuning method and a fixed-shunt tuning in terms of the robustness to parametric uncertainty, and in practical terms for realisation using analogue or digital shunt impedances.

Keywords:
vibration control, metamaterial, adaptive, robust, uncertainties, shunt

1. Introduction

Tuned Vibration Absorbers (TVAs) have been used for many years to control unwanted structural vibration. However, these narrow-band devices are limited to absorbing vibration around their tuning frequency [1]. Therefore, they are only effective in controlling modal vibration if the tuning frequency corresponds with the resonance frequency of the structural mode. Parametric uncertainty or changes to the system over time can therefore render TVAs ineffective due to changes in the structural modes. Multiple TVAs with resonance frequencies distributed around a target frequency can improve robustness, as well as increasing the attenuation at the nominal target frequency [2].

An alternative approach to achieving robustness to structural uncertainties is the use of tuneable resonators, where the response of the resonators can be changed or varied in order to more effectively control the observed vibration response of the structure. Tuning the resonance frequency of a vibration absorber by mechanically varying the geometry of a stiffness element has been widely demonstrated [3, 4, 5]. However, any control elements (mechanical actuators, sliding parts) add to the footprint of the device, the complexity of the design, and introduce more components that can fail. Smart materials exhibit a change in their material properties in the presence of a change in their environment, and have also been used to develop variable stiffness vibration absorbers. Examples of smart materials used to produce variable stiffnesses include: Magnetorheological and Electrorheological Fluids (MRFs/ERFs) [6, 7]; Magnetorheological and Electrorheological Elastomers (MREs/EREs) [8, 9]; and Shape Memory Alloys (SMAs) and Polymers (SMPs) [10, 11]. However, these smart materials exhibit complex dynamics and other drawbacks such as particle sedimentation (MRF/ERFs) and relatively slow response times (SMA/SMPs). The smart materials most commonly utilised in tuneable resonators are piezoelectric elements [12, 13, 14], which produce a mechanical stress in the presence of an electrical charge that can be used to deform or resist the deformation of a stiffness element in order to modify its stiffness. Because piezoelectric elements are reciprocal transducers, the electrical charge transduced when a stress is applied to the element can be conducted back through the element to transduce an opposing stress. This is known as "shunting", and by placing an impedance circuit in series with the piezoelectric element, the stiffness and damping of the element can be tuned [15], and internal resonances can be introduced [16] to create resonant absorbers. In [17, 18, 19] an elastic metamaterial (EMM) consisting of an array of electrically shunted piezoelectric patches has been used to adaptively control the vibration of a beam or plate. Piezoelectric patches are used to exert a bending force on the host structure, and can be used as resonant absorbers without a proof-mass. However, because they exert a bending force rather than a translational force, they are limited to resonant absorption of flexural motion when used in this way.

The use of a shunted electrodynamic inertial actuator as a variable damping vibration absorber has been explored in [20] and has been shown to require lower shunt voltages than piezoelectric actuators and can exert a larger force. Voice coil actuators tend to be lower cost than piezoelectric equivalents, and readily available "off-the-shelf" in a wide range of sizes and masses. Paulitsch et al. furthered this research in [21], investigating voltage and current feedback control of a resistance and capacitance shunted device to dampen vibration of a SDOF structure. In [22], matching the resistance and inductance of the actuator coil and cancelling them out with a negative impedance shunt is shown to considerably attenuate the first four modes of vibration in a plate. To tune the resonance frequency of a proof-mass electrodynamic actuator, the effective stiffness can be varied through the use of a negative resistive and capacitative shunt impedance [23]. The derivation of the mechanical equivalents of parallel resistor and inductor shunt branches is later set out in [24] where, provided the resistance and inductance of the actuator coil are cancelled by an equal negative impedance, a resistor can be shown to act as a mechanical damper and an inductor as a mechanical stiffness, with the effective stiffness and damping values a product of the inverse of the component impedance and actuator transduction coefficient. In a later study from the same authors [24], a series resistive and inductive (RL) shunt is used instead, which does not require full cancellation of the coil inductance and resistance, to sweep the tuning frequency between bounds in order to achieve wide-band vibration control of a cylinder [25]. Many of the studies into adaptive shunting implement the variable impedance digitally. This allows greater flexibility and control, however, there are drawbacks. A digital synthetic shunt impedance was first proposed in [26], using three operational amplifiers to allow the connection of a digital voltage filter implementation of the required impedance. However, digital synthetic shunting requires a very high sampling frequency to avoid latency issues [27], and therefore the computational requirements for a large array of devices would be high. Alternatively, a matrix-switched bank of circuits could be designed to allow the selection of discrete tuning frequencies for each resonator on a very small scale, with the only computational cost being setting or computing the tuning frequencies required.

Traditional TVAs are bulky and heavy, and exert localised control forces on the structure being controlled. Thin and lightweight structures may not be able to support such large, localised forces, and, therefore, alternative lightweight distributed vibration control solutions are required. Metamaterials offer one potential solution to this challenge. Metamaterials exhibit unusual effective material properties, through the arrangement of substructures that are much smaller than the wavelength of vibration [28]. Elastic Metamaterials (EMMs) interact with elastic waves in solids, and can be distributed over a structure, therefore also distributing the control force. Although EMMs can interact with waves in a number of ways, this study focuses on their ability to absorb vibration through local vibrational resonances within the periodic substructures making up the EMM. Early locally-resonant metamaterial vibration absorbers demonstrated that the absorption occurs when the motion of the mass of the substructure opposes the motion of the structure [29], and that for flexural vibration this motion must be translational rather than rotational [30]. Multi-mode vibration control has been demonstrated through the integration of differently tuned resonant substructures into rods [31] and plates [32], with the former also showing that a broader band gap can be achieved by distributing the tuning frequencies of the metamaterial substructures over a range of frequencies, similar to the work on TVAs presented in [2]. In [17, 18, 19] the concept of tuneable, shunted piezoelectric patches has been applied to an EMM, with an array of electrically shunted piezoelectric patches used to adaptively control the vibration of a beam or plate.

This paper presents an electrodynamic metamaterial unit cell, consisting of multiple shunted inertial electrodynamic actuators, and an adaptive tuning approach, whereby the resonance frequencies of the unit cell are changed in real-time, based on analysis of the structural response. The proposed adaptive electrodynamic metamaterial (AEDMM) utilises variable shunts to modify the resonance frequencies accordingly. The adaptive shunting method is compared to a "blind sweep" tuning approach in terms of nominal and robust performance, using time-domain simulations. It is proposed that analogue switching circuits with a single central controller would be more practical for large arrays of resonators than digital synthetic impedances. Therefore, the two approaches are also compared in terms of their ease of realisation using analogue circuitry. Readily available actuators at the proposed scale are only capable of producing very small voltages (± 30 mV) within the linear dynamic range, and the variation in the electrical and mechanical parameters in these actuators is quite high. Therefore, experimental validation of the work in this paper would require significant work designing low-noise, high efficiency electronic circuits. Vibration control using both fixed [33] and time-varying [25] shunted electrodynamic actuators has previously been demonstrated with good agreement between simulation and experimental implementation. Simulation studies have been demonstrated as effective evaluation techniques for vibration control systems even in complex time-varying structures [34]. This paper presents the results of simulation studies only, and these are considered sufficient to analyse the differences between the control methods under investigation. Firstly, the effect of shunting on an electrodynamic actuator is examined. The proposed EMM is then set out, along with an example modal structure for evaluation of the EMM's performance. The different tuning approaches investigated are described, before an investigation into the configuration of the tuning approaches is carried out. The different tuning approaches are then evaluated and compared in terms of their performance on a nominal structure, and on a structure with parametric uncertainty. Finally, the different tuning approaches are evaluated and compared for their performance in the presence of uncertainty in the mechanical properties of the actuator.

2. A shunted inertial electrodynamic actuator

Before considering different tuning approaches, the effect of a parallel resistive-inductive (RL) and resistive-capacitive (RC) shunt on an inertial electrodynamic actuator was first examined. This section sets out the theory behind the shunt approach, and describes how the shunt can be tuned to achieve a certain resonance frequency and damping ratio.

The effect of a parallel RL shunt circuit on an inertial electrodynamic actuator has been well examined in the literature. Turco and Gardonio [24] demonstrated that the equivalent mechanical impedance, Z_{me}, produced by a shunted idealised coil-magnet two poles element, is equal to $(Bl)^2/Z_s$, where Bl is the transduction coefficient and Z_s is the shunt impedance. An RLC parallel shunt has the total electrical impedance

$$Z_s = \left(\frac{1}{R_s} + \frac{1}{\mathrm{j}\omega L_s} + \mathrm{j}\omega C_s\right)^{-1}, \tag{1}$$

and therefore the equivalent mechanical impedance

$$Z_{me} = (Bl)^2\left(\frac{1}{R_s} + \frac{1}{\mathrm{j}\omega L_s} + \mathrm{j}\omega C_s\right). \tag{2}$$

A resistance and inductance in parallel therefore present an additional effective damping and stiffness respectively (as shown in [24]), provided the impedance of the coil is cancelled out with a negative impedance, whereas a capacitance can be represented as an additional effective mass. Figure 1 shows an actuator shunted by a parallel resistance R_s, inductance L_s, and capacitance C_s. A negative resistance and inductance are also included to cancel out the impedance of the coil. Figure 1 also shows the equivalent mechanical-only representation.

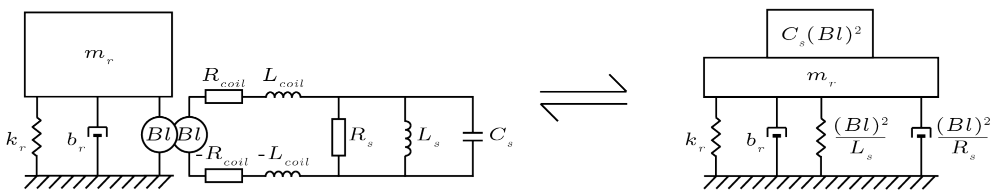

Figure 1: Mechanical-electrical diagram (left) and equivalent mechanical diagram (right) of an ideal shunted electrodynamic inertial actuator with: moving mass, m_r; suspension stiffness, k_r; damping, b_r; transduction coefficient, Bl; voice coil resistance, R_{coil}; voice coil inductance, L_{coil}; shunt resistance, R_s; shunt inductance, L_s; and shunt capacitance, C_s.

Assuming simple harmonic motion, and that all component values are constant and independent of frequency and displacement over the considered range, the equation of motion for the system set out in Figure 1 can be expressed as [24]

$$F(t) = (m_r + C_s(Bl)^2)\ddot{w}_r(t) + \left(b_r + \frac{(Bl)^2}{R_s}\right)\dot{w}_r(t) + \left(k_r + \frac{(Bl)^2}{L_s}\right)w_r(t), \tag{3}$$

where $F(t)$ is the driving force acting on the mass, w_r is the displacement of the mass, and the remaining terms are defined in Figure 1. The receptance, $\alpha(\omega)$, is equal to the displacement per unit force, or $\frac{W_r(\omega)}{\tilde{F}(\omega)}$. Assuming $F(t) = \tilde{F}e^{\mathrm{j}\omega t}$ and $w(t) = We^{\mathrm{j}\omega t}$, this can be expressed as

$$\alpha(\omega) = \frac{W_r(\omega)}{\tilde{F}(\omega)} = \frac{1}{-\omega^2(m_r + C_s(Bl)^2) + \mathrm{j}\omega(b_r + \frac{(Bl)^2}{R_s}) + (k_r + \frac{(Bl)^2}{L_s})}. \tag{4}$$

The magnitude peak of the receptance falls at the resonance frequency of the system, and this occurs when $(k_r + \frac{(Bl)^2}{L_s}) - \omega^2(m_r + C_s(Bl)^2) = 0$. The solution to this gives the closed-circuit resonance frequency, $f_{r,\,c}$, where $f_{r,\,c} = \omega_{r,\,c}/2\pi$, which can then be expressed as

$$f_{r,\,c} = \frac{1}{2\pi}\sqrt{\frac{k_r + \frac{(Bl)^2}{L_s}}{m_r + C_s(Bl)^2}}. \tag{5}$$

From equation 5 it can be seen that the effective stiffness increases as L_s decreases and the effective mass increases as C_s increases. For simplicity in tuning the resonators, it is assumed that for $f_{r,\,c} > f_{r,\,o}$, where $f_{r,\,o}$ is the open-circuit resonance frequency, the capacitance is switched out of the circuit and for $f_{r,\,c} < f_{r,\,o}$ the inductance is switched out of the circuit. The required values of L_s and C_s to achieve a desired resonance frequency can therefore be expressed as

$$L_s = \frac{(Bl)^2}{\omega_{r,c}^2 m_r - k_r}; \tag{6}$$

$$C_s = \frac{k_r - \omega_{r,c}^2 m_r}{(Bl)^2\omega_{r,c}^2}. \tag{7}$$

The actuator damping ratio ζ_r, can be expressed as

$$\zeta_r = \frac{(Bl)^2 + b_r R_s}{2\omega_{r,c} m_r R_s}, \tag{8}$$

and for a desired damping ratio of ζ_r, the required R_s can therefore be expressed as

$$R_s = \frac{(Bl)^2}{2\zeta_r\omega_{r,c}m_r - b_r}. \tag{9}$$

R_s can become negative when $b_r > 2\zeta_r\omega_{r,c}m_r$, which can occur at very low frequencies. In order to maintain the simplicity of the shunt impedance, this is considered undesirable. To ensure a positive value for R_s, the b_r term is neglected and Eq. (9) becomes

$$R_s = \frac{(Bl)^2}{2\zeta_r\omega_{r,c}m_r}. \tag{10}$$

This removes the possibility of R_s becoming negative, but the calculated value for R_s cannot accurately produce the specified damping ratio ζ_r. The actual damping ratio will be much higher at low natural frequencies of the shunted resonators (for example, for $\zeta_r = 0.01$, the actual damping ratio at 10 Hz is 0.19 and at 100 Hz is 0.03). Because of this, attenuation at low frequencies will likely be reduced, but this modified formula avoids the complications due to a negative shunt resistance, such as instability.

Equations 6, 7 and 10 are used to calculate the required component values to achieve the specified resonance frequency and the approximate damping ratio defined by the tuning approaches examined in the following section.

3. A tuned-shunt electrodynamic metamaterial

This section sets out the proposed electrodynamic metamaterial (EDMM) for the attenuation of multiple modes of structural vibration. An example structure is described, and the EDMM system defined, including a description of the different tuning approaches being investigated. These approaches will then be compared in terms of their effectiveness and ease of implementation using simulation studies in the following sections.

3.1. Example structure

A nominal three degree-of-freedom, mass-spring-damper system with a fixed base is used to evaluate the performance of an attached EDMM. The EDMM, consisting of 12 single-degree-of-freedom (SDOF) individually-shunted, electrodynamic resonators, is connected to the free, top mass as shown in Figure 2. Having only a single unit cell and three degrees of freedom in the structure keeps the computational demands on the time-domain simulation to a reasonable level, while still providing clear insight into the EDMM performance.

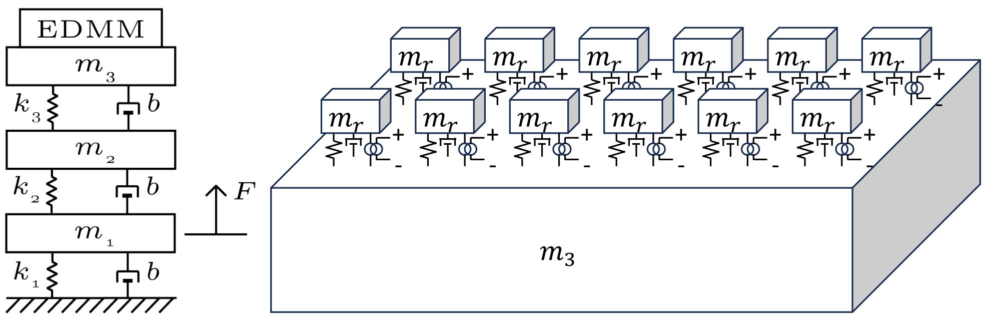

Figure 2: Left: Structure and EDMM used in the simulation study. Right: EDMM attached to the structure.

A miniature electrodynamic actuator, the Tectonic Audio Labs TEAX09C005-8, has been previously characterised by the authors in [35], and so the mean characterised parameter values for this actuator are used for the EDMM in this study. The total mass of the structure was set such that the mass of the EDMM unit cell equates to 20% of the structural mass, and this mass is divided equally between masses $m_{1,\,2\ and\ 3}$. The stiffness values $k_{1,\,2\ and\ 3}$ were then set to provide three modes of vibration within the frequency range of 5–500 Hz. The response of the structure is damped with a viscous damping model with damping coefficient, b of 0.1 Nsm^{-1}.

3.2. EDMM Tuning approaches

This paper proposes a novel adaptive EDMM tuning approach to achieve robust attenuation of vibration. In order to evaluate the performance of this approach it is compared to two alternative tuning approaches: a fixed tuning, based on the resonance frequencies of the nominal structure; and a blind-sweep, similar to the approach set out in [24]. The three approaches are detailed as follows.

3.2.1. *Fixed tuned shunts*

The fixed-tuning approach used here is a 'low-intelligence' approach and is included to provide a simple benchmark for the performance of the other methods in this study. For this study, the tuning frequencies of the 12 fixed tuning shunted resonators are distributed equally between the three modes of the nominal structure (4 resonators are tuned to each modal frequency), with no consideration for the energy at each mode or an attempt to define an optimal distribution. The modal frequencies are calculated with the addition of the resonators, therefore taking into account the shift in the resonance frequencies caused by their addition to the structure. Although an optimal fixed tuning approach could be used to provide improved performance, particularly in the presence of uncertainties [35], this is not considered here since it requires additional a priori information about the structure and its uncertainties.

3.2.2. *Discretised swept shunts*

Wide-band absorption from a shunted electrodynamic resonator was demonstrated in [24] and [36] using a digital synthetic impedance to produce a continuous squared cosinusoidal sweep of the resonance frequency between upper and lower bounds. Further, in [37] it was shown that for a shunted piezoelectric patch that the attenuation achieved when the shunt was switched synchronously through the resonance frequencies of the structure was comparable to a continuous sweep across a bandwidth in which the structural modes were contained. A discrete number of sweep frequencies would be more realistically achievable than a continuous sweep when using a switching analogue circuit, and so a discretised sweep is the approach taken in this paper. The studies in [24] and [36] also demonstrated how the optimal sweep period, T, is dependent on the modal frequencies of the structure. Investigating the optimal period is not considered at this stage, but this could form part of a future study. In this paper, a time period of $T = \frac{1}{14}$ s is used, which is of the same order as that discussed in [24] and [36]. This means that the resonance frequency of the actuator is swept over the defined frequency range a total of 28 times per second.

The lower the resolution of the discretised sweep, the fewer the number of different tuning frequencies, and the lower rate of switching. For a switching analogue circuit, keeping this number low is advantageous in that it not only reduces the number of components and therefore the size and complexity of the circuit required, but it reduces the load on switching components, potentially extending the life of the system. However, the spacing between adjacent frequencies in the sweep, and their distribution with relation to the structural resonance frequencies is likely to affect performance. The effect of the resolution of the sweep has therefore been investigated with a parametric study. Also considered in this study is whether any change in performance is seen if there is an offset in the resonance frequencies (or asynchronicity between the resonance frequencies of the shunted actuators) when multiple actuators with swept tuning are used. As well as the potential for a change in performance, such as that seen with multiple tuned vibration absorbers in [2], the effect of any offset between resonance frequencies would also determine whether multiple actuators would need to be controlled as one, or synchronised using a clocking signal, to guarantee performance. The effect of asychronicity of varying magnitude is also investigated using a parametric study.

3.2.3. *Novel adaptive switched shunts*

The performance of fixed tuned shunts is known to be limited, particularly when there are changes in the structure, and careful design is thus required based on assumed prior knowledge of the structure to optimise the tuning frequencies. In this study, to overcome the limitations of fixed tuned shunts, a novel adaptive shunted electrodynamic metamaterial (AEDMM) is proposed. The proposed adaptive tuning algorithm uses real-time spectral analysis of the structural response to tune the resonators in the EDMM to the frequencies with the greatest energy.

To do this, the velocity of m_3, $\dot{w}_3$ is sampled at a rate of f_s Hz. This signal is stored in a buffer of length NFFT, and every n_{update} samples the contents of this buffer, $\bar{W}$, is passed to a fast-fourier transform (FFT) calculation. The FFT uses a logarithmic frequency vector in order to more evenly distribute the frequency bins around each modal peak. The FFT outputs a single-sided complex frequency spectrum, $\bar{X}$, and the corresponding vector of frequencies, $\bar{F}$. The frequency vector, $\bar{F}$ is then sorted in order of descending magnitude of the corresponding spectra, $\bar{X}$. The sorted frequency vector, $\bar{F}_{sort}$, is truncated to the first N values, therefore the N highest magnitude response frequencies and the desired closed-circuit resonance frequencies of the EDMM unit cell, $\overline{F_{r,c}}$. Using equations 6, 7 and 10 the component values of the RLC parallel shunt are calculated. When the desired resonance frequency is less than or equal to the open-circuit resonance of the electrodynamic actuator ($\overline{F_{r,c}}[n] \leq f_{r,o}$), the capacitor branch is switched in and the inductor branch is switched out. When $\overline{F_{r,c}}[n] > f_{r,o}$ the capacitor branch is switched out and the inductor branch is switched in. This algorithm is set out step-by-step in Algorithm 1 below, and in Figure 3.

Algorithm 1: adaptive tuning

Input: $\dot{w}[n]$, structural velocity measured at a single position

Output: R_s, L_s, C_s

1. Calculate frequency domain response using a logarithmically distributed FFT of length NFFT (samples).
2. Sort frequency vector in descending order of frequency response magnitude.
3. Truncate frequency vector to first N (corresponding to the N highest magnitudes).
4. Calculate required R_s, L_s and C_s values to achieve selected tuning frequencies and damping ratio.
5. Implement new component values.
6. Hold for an update period of length n_{update} (samples).
7. Repeat

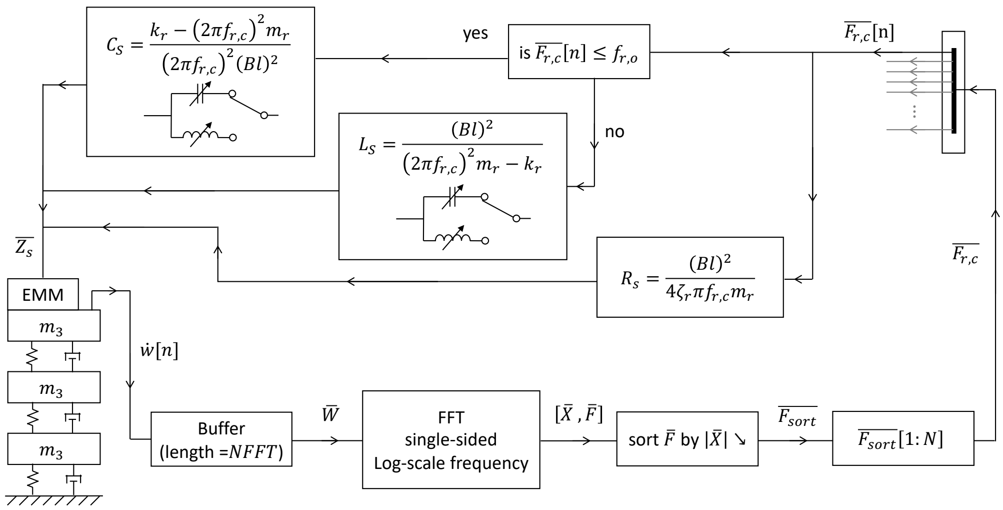

Figure 3: Block diagram of proposed adaptive tuning algorithm.

Two parameters must be specified to configure this tuning approach: NFFT, and n_{update}. The length of the FFT will correspond to the number of frequency bins and therefore the resolution of the frequency selection process. This will have a significant effect on the performance, as it directly affects the distribution of the tuning frequencies, and how closely the possible tuning frequencies align with the structural modal frequencies. The rate at which the tuning frequencies are updated may also have an effect on performance. Both of these parameters have therefore been investigated using parametric studies, and the results will be described in the following section.

4. Simulation Methodology

This section sets out a simulation configuration that is used to investigate the performance of the tuned-shunt electrodynamic metamaterial approaches described in the previous section. The method of simulation is first set out, and then the results of initial convergence studies carried out to investigate the effect of different parameters on each approach are discussed. This includes the effect of the EDMM on the modal resonances in order to effectively design the fixed-tuning EDMM.

4.1. Simulation setup

The three degree-of-freedom structure shown in Figure 2 has been simulated, with a disturbance force consisting of band-limited white noise applied to m_1. The shunted inertial actuators are modelled as SDOF mass-spring-dampers with a shunted magnet-coil assembly between the mass and the host structure. All simulations were carried out using MATLAB/Simulink and the Simscape library of mechanical and electrical component blocks. Simulink automatically selects a suitable solver: “ode45” (Dormand-Prince pair method [38]) is selected for the structure without the EDMM; “ode23t” (modified trapezoidal rule [39]) is selected for the structure with the EDMM. A simulation time of 300 s was maintained throughout all simulations.

4.2. Selection of Fixed-Tuning Resonance Frequencies

As described in Section 3.2.1, under the fixed-tuning approach, the 12 resonators in the EDMM are divided equally between the three modal frequencies. The modal frequencies of the structure can be modelled or measured relatively straightforwardly, and so it is assumed that they can be determined in advance. However, the addition of the EDMM, which has a mass equal to 20% of the mass of the structure, will have an effect, shifting the modes down in frequency. The structure was therefore simulated with and without the EDMM attached, with the EDMM initially simulated in an open-circuit state, with no shunt impedance. Figure 4 shows the mobility FRF magnitude and phase of m_3 for both cases. It can be seen that there is a slight downward shift in all three modes. The third mode is reduced in amplitude quite significantly, which is expected, due to the increased force required to move the additional mass introduced by the EDMM. The random phase seen above the third modal frequency is due to mechanical shock introduced by instantaneous changes in the shunt impedances. The resonance frequencies with the EDMM included are observed at 18.3 Hz, 103.5 Hz and 322.5 Hz. The fixed-tuning shunted EDMM therefore has 4 of the 12 resonators tuned to each of these frequencies.

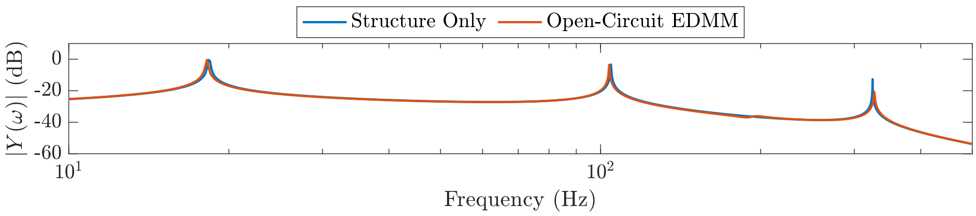

Figure 4: Mobility FRF magnitude of m_3, with and without the open-circuit EDMM.

4.3. Selection of Discretised Sweep Parameters

The effect of a discretised swept tuning will likely depend on the resolution of the sweep, and the sweep time period. In addition, for multiple swept tuning resonators, there may be a change in performance depending on whether the resonators are all swept synchronously or asynchronously with an offset in the tuning frequency between each actuator. This section sets out an investigation into the selection of these parameters. The squared-cosinusoidal sweep pattern is investigated with a wide range of resolutions, from 100 discrete frequency values, to 1140 discrete frequency values. In addition to varying the sampling frequency, the effect of asynchronously sweeping the 12 resonators in the EDMM has been considered. In this case, the resonance frequencies of the 12 resonators at time t are equally distributed across a range of the sweep. The range is defined by a Normalised Offset of between 0 and 1, where 0 represents a synchronous sweep and 1 represents a distribution spanning the half-cosine period $T/2$, where the sweep offset in seconds, t_{offset}, for 12 resonators is $T/24$.

A convergence study comparing both the sweep resolution, SR, and the effect of the Normalised Offset between the resonators has been carried out. Figure 5 shows a plot of the resulting $E_{k,atten}$ over the frequency range of interest. Crosses mark instances where the simulation has failed. This seems to be when either there is an instability, causing the voltages in one or more shunt circuit to rise uncontrollably, or when there is a significant step change in voltage such that the solver used does not converge. It is known that a step change in impedance (such as that induced by a discretised, switching tuning approach) causes a step change in electrical current and therefore introduces noise into the system. Initial investigation has shown that there is a relationship between the current frequency and the rate at which the shunt is switched which causes resonances in the electrical circuits, exacerbating the noise problem and potentially causing instability and large voltage spikes. However, further investigation is required to clearly identify these relationships, which will form part of future work. It is clear from the vertical banding in Figure 5 that the two parameters are unrelated and can therefore be considered independently. The total range in $\bar{E}_{k,\ atten}$ is less than 0.5 dB, with the highest performing SR falling at SR = 1060. It is possible that as the resolution becomes comparable to a true continuous sweep that the performance will converge, but simulating higher resolutions than these will increase computational demands further and no significant benefit is expected. These results suggest that the discretisation of the sweep may result in instability and/or large voltage spikes and therefore knowledge of the system response in the design stage is important.

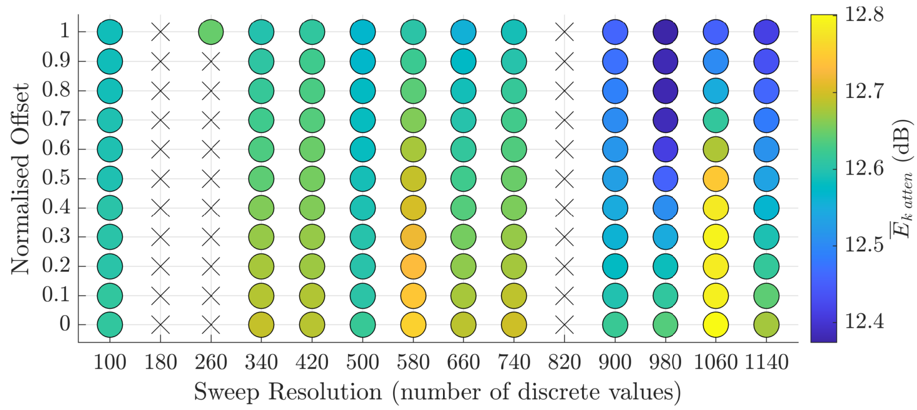

Figure 5: Plot showing the attenuation in the kinetic energy provided by the discretised sweep EDMM for different sweep resolutions and resonator tuning frequency offset. The crosses indicate where the system response is either unstable or unsolvable.

4.4. Selection of Adaptive Switched Algorithm Parameters

The adaptive algorithm relies on structural feedback. It is proposed that the required sensing is collocated with the EDMM mounted to the top mass of the structure (m_3). Figure 4 shows that m_3 has peaks in the dynamic response at each structural mode, and there are no anti-resonances, making it suitable for analysing the structural response.

As the adaptive switched algorithm selects the tuning frequencies based on the frequency bins of the FFT, the length of the FFT (NFFT) will have a strong influence on which points are selected, and the rate at which the algorithm updates the component values (n_{update}) may also affect the performance of the adaptive EDMM. As the FFT is symmetrical, the number of discrete tuning frequencies available for the adaptive algorithm is equal to NFFT/2. Figure 6 shows the broadband attenuation of the kinetic energy of the top mass, $\bar{E}_{k,\ atten}$, for different values of NFFT/2 and n_{update}. The crosses that occur at low values of NFFT/2 and n_{update} correspond to failures in the Simulink solver, which seem to be a result of large voltage spikes being induced by the switching of impedances. For low values of NFFT/2 the steps between tuning frequencies, and therefore shunt impedances, are larger, and when updated more frequently it is hypothesised that this is more likely to introduce significant voltage build ups. From this convergence study, the highest levels of attenuation are achieved with NFFT/2 = 2^{11}. However, if the system is to be implemented with a switching analogue shunt, as proposed, then a small number of possible tuning frequencies is desirable. The difference in performance between the configurations with n_{update} = 2^9 and NFFT/2 between 2^6 and 2^{11}, is less than 3 dB. Therefore the practical benefit of the low number of tuning frequencies may outweigh the performance benefit.

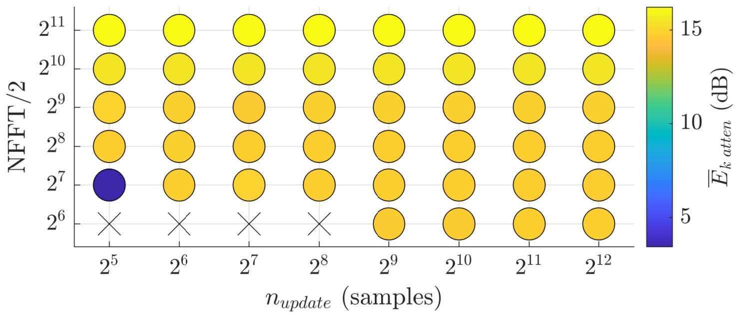

Figure 6: Contour plot showing the attenuation in the kinetic energy provided by the AEDMM for different FFT lengths and update rates. The crosses indicate where the solver failed.

5. Nominal performance

Using the simulation configuration set out in the previous section, the performance of the EDMM on a nominal structure was first investigated. Two adaptive and two swept configurations are compared:

- a "low resolution" adaptive configuration with NFFT/2 = 2^6 and n_{update} = 2^9;
- a "low resolution" sweep that is discretised to the same number (SR = 2^6) of possible tuning frequencies;
- a "high resolution" sweep taken from the highest performing configuration in the convergence study, with SR = 1060;
- a "high resolution" adaptive configuration with a corresponding NFFT/2 = 1060.

By selecting configurations with identical numbers of tuning frequencies in both approaches, a direct comparison can be made in terms of performance. Figure 7 shows the mobility FRF for all discussed cases: the structure alone, fixed-tuning EDMM, and the aforementioned configurations of the adaptive and swept tuning approaches. Due to the overlapping responses, the mobility is separated into bandwidths around each mode for clarity. The response outside of these ranges is insignificant and therefore excluded to better highlight the regions of interest. It can be seen from Figure 7 that the fixed-tuning achieves a dip in the response at the frequencies where the resonators of the unit cell have been tuned, but that this dip has small peaks either side of it. This is expected as it has been well examined in research into traditional TVAs. The side peaks produced are, in all frequency bands shown, higher in magnitude than the peak response for the other tuning approaches, despite achieving high attenuation of the structural response. The two swept configurations perform very similarly, with the lines barely distinguishable from each other bar a difference in the noise displayed in the highest frequency band. This low level noise is induced by the rapidly switching shunt circuit, as the step change in impedance causes a similar change in the current flow. This noise is not visible in the adaptive approaches. Noise is induced, which can be seen if the mobilities are evaluated without time averaging, but it is much lower level. This is because the adaptive approaches switch every 32 ms, compared to the swept approaches which switch every 1 ms (low resolution) or every 67 μs (high resolution). Both adaptive methods achieve greater attenuation than the swept in all frequency bands, with the high resolution adaptive method achieving a marginally greater attenuation of the first mode. From evaluating what tuning frequencies are selected during the simulations, it is seen that in the high resolution adaptive approach, all resonators are consistently tuned around the first mode, whereas in the low resolution approach the resonators are distributed over the first two modes, but with the majority tuned around the first mode. The reason why the second and third modes are still well controlled is likely in part due to the additional effective mass presented by the RC shunt when tuning the actuator resonance frequency to one below its open-circuit resonance, but also due to the increase in damping ratio at low tuning frequencies caused by the modification used to calculate the shunt resistor value (Equations 9 and 10), as discussed at the end of Section 2.

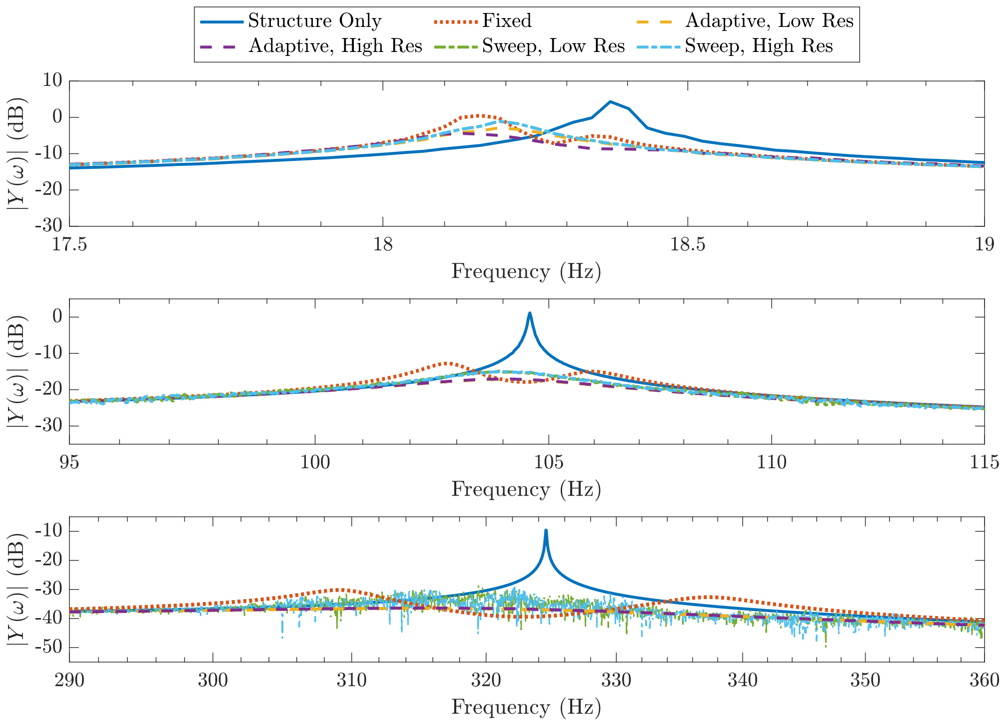

Figure 7: Mobility FRF magnitude, of mass m_3, for the different shunted EDMM tuning methods over frequency bandwidths around the first (top), second (middle), and third (bottom) structural modes.

Table 1 shows the reduction in the peak mobility magnitude of the top structural mass (m_3) achieved by each tuning approach, in each of the three frequency bands shown in Figure 7, alongside $\bar{E}_{k,\,atten}$ for the whole frequency range of interest. It is clear from these results that the adaptive approaches achieve greater attenuation than the fixed and swept approaches, in both attenuation of each individual mode and the mean attenuation of energy. Because of the noise around the third mode in the swept approach, it actually achieves poorer reduction in the peak mobility than the fixed tuning.

Table 1: Peak-to-peak reduction in each modal frequency band and attenuation in kinetic energy achieved by each tuning method.

Tuning	**Band-limited reduction in peak $\lvert Y(\omega)\rvert$ (dB)**			
Method	**17.5-19 Hz**	**95-115 Hz**	**290-360 Hz**	$\bar{E}_{k,\,atten}$ **(dB)**
Fixed	3.8	13.9	20.6	10.8
Sweep, Low Resolution	5.4	16.2	19.1	12.7
Sweep, High Resolution	5.4	16.2	18.9	12.7
Adaptive, Low Resolution	7.2	18.3	26.9	14.7
Adaptive, High Resolution	8.7	18.2	26.8	11.7

Consideration of the time-averaged response alone is not sufficient to judge the effectiveness of any of these approaches, as dynamics that vary over time will result in variation in the response over time. Large spikes in the velocity response of the structure, or a 'pulsing' of modes would not necessarily be shown in the time-averaged response but could be equally undesirable. The variation in the velocity response over time is therefore also considered, since it may provide useful insight into the performance of the different approaches. Figure 8 shows the peak of the magnitude-squared velocity STFT of the top mass over time, from the total frequency range of interest (5–500 Hz) and in each of the three modal frequency bands (17.5–19 Hz, 95–115 Hz and 290–360 Hz) defined previously, for the structure, fixed tuning, and low resolution adaptive and swept approaches. The first 20 seconds are omitted to allow the structural response to reach steady-state. Comparing these results corresponding to the total frequency range and in each of the modal frequency ranges, it is clear that the overall response is dominated by the first mode. The adaptive and swept approaches achieve a consistent level of attenuation over the full frequency range, however, the fixed tuning sweep seems to cause an enhancement in the first mode at around 170 s. This is an undesirable attribute and casts doubt over the suitability of this as a tuning method even for a nominal structure. The peak velocity over time shown in Figure 8 is smoothed due to the windowing used to calculate the STFT, so impulsive spikes would not be visible. However, analysis of the time domain data shows that there are no significant spikes in the velocity of the structure caused by any of the tuning approaches. The switching noise previously observed in the highest modal bandwidth is masked in the overall response plot due to the dominance of the first mode and is of relatively low amplitude and therefore low concern.

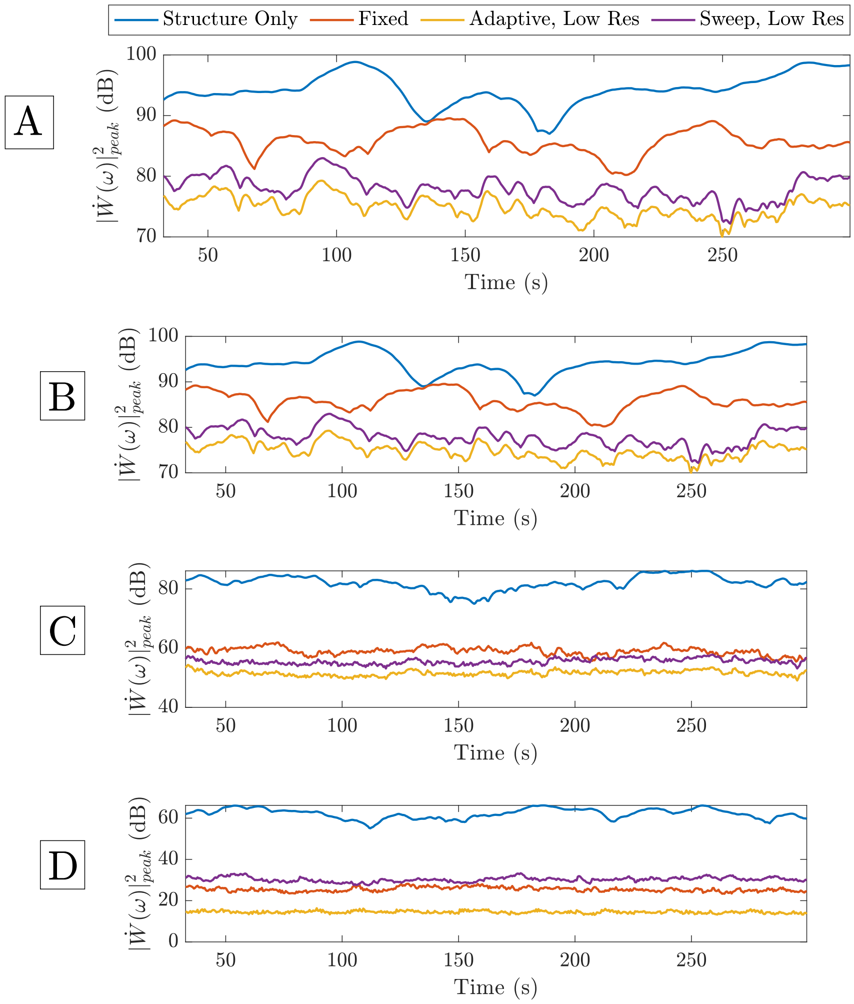

Figure 8: Peak magnitude-squared velocity STFT over the total frequency range of interest (A) and in the different modal frequency bands (B = 17.5–19 Hz; C = 95–115 Hz; D = 290–360 Hz)

6. Robust performance

In the previous sections, a nominal structure has been considered with fixed parameters. In practice, there are likely to be uncertainties in the system, and this could affect the performance of the tuning approaches. In this section, the robustness of the previously described tuning approaches are investigated when they are applied to a structure with parametric uncertainty. In addition to uncertainty in the structure, uncertainties in the mechanical parameters of the actuators are also considered. However, uncertainty in the actuator electrical characteristics is not considered, since using the proposed parallel shunt method to modify the dynamic response of the actuators requires their electrical impedance to be completely cancelled out and uncertainties would negate the effect of the shunt. In practice, any variation in the electrical characteristics of the actuator would need to be identified using thorough measurement or a self-tuning approach.

The primary metric used to assess robustness in this study is the mean attenuation in the kinetic energy over multiple uncertain cases. The standard deviation in the attenuation in the kinetic energy is also presented, along with the highest and lowest attenuation achieved in the range of results. This is because poorly performing outliers are of significant interest when the system is unknown, and the range of results along with the standard deviation gives an idea of the spread in performance.

In the previous section, an investigation into the effect of the various parameters used in the different tuning approaches was presented. Although this could be repeated to find the optimal parameters for robust performance, this would be extremely time consuming and would require prior knowledge of the type of uncertainty. Therefore, the same investigation has not been carried out for the robustness study. Initially, it was proposed that the same configurations used to compare the nominal performance of each approach would be used to compare the robust performance. However, it was subsequently found that the low resolution adaptive approach and both configurations of the swept approach suffered from voltage spikes and instabilities when applied to the uncertain cases. Through trial and error it was found that increasing the period of the sweep from 1/14 s to 1/4 s reduced the rate of switching sufficiently to avoid the issues caused by the impedance changes. This reduction in switching rate also has the benefit of making the swept tuning more practical for implementation in analogue. The update rate of the low resolution adaptive configuration was increased from 2^9 to 2^{10} in order to have the same effect. Therefore, this modified set of configurations was used to assess the robust performance. It was seen in the convergence study on the adaptive approach that increasing the update rate had a minimal impact on performance. However, it is unknown what effect the increase in sweep period will have on the nominal performance, and this will need to be considered as part of the robust evaluation.

6.1. Structural Uncertainties

In order to produce uncertainties in the modal frequencies of the structure, the stiffness components of the three degree-of-freedom structure were subject to random variation, with a normal distribution. The simulation was run for the nominal structure and for 50 additional structures where each stiffness component was set to a new value between ±50 % of the nominal value. This range constrains the structural resonance frequencies to a frequency range of 5–300 Hz. These values were chosen in advance of all simulations using a random number generator and the same set of uncertain structures was used with each tuning approach to provide a consistent comparison. Figure 9 shows the mobility FRF magnitude of the top mass with no EDMM for the nominal structure (solid line) and for all cases with structural uncertainty (bounded by dashed line). The significant shifts in the modal frequencies of the structure in the presence of uncertainty can clearly be seen.

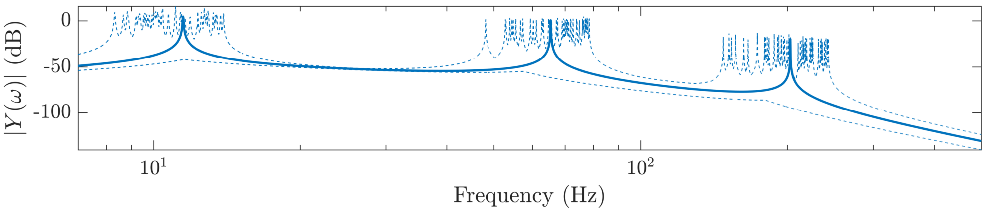

Figure 9: The mobility FRF magnitude of the top mass of the structure for the nominal case (solid line) and for all cases with structural uncertainty (bounded by dashed lines).

The simulated velocity of the top mass, with and without the EDMM attached, was used to calculate the mean broadband attenuation in the kinetic energy, $\bar{E}_{k,\,atten}$, achieved by the different tuning approaches. The robustness is examined in Figure 10 using the four robustness metrics defined above. From Figure 10 it can be seen that the mean attenuations achieved by the adaptive and swept methods far exceed that achieved by the fixed EDMM. It can also be seen how both adaptive configurations outperform both swept configurations in all metrics. The high resolution approaches only marginally outperform their low resolution counterparts, meaning that the benefit of a small number of shunt circuits in an analogue realisation would probably be a more important factor in the design of the system. The fixed tuning is, as expected, demonstrated to be completely unsuitable for robust control, by the only marginally positive $\bar{E}_{k\ atten}$, and a positive value for minimum attenuation indicating enhancements in at least one case.

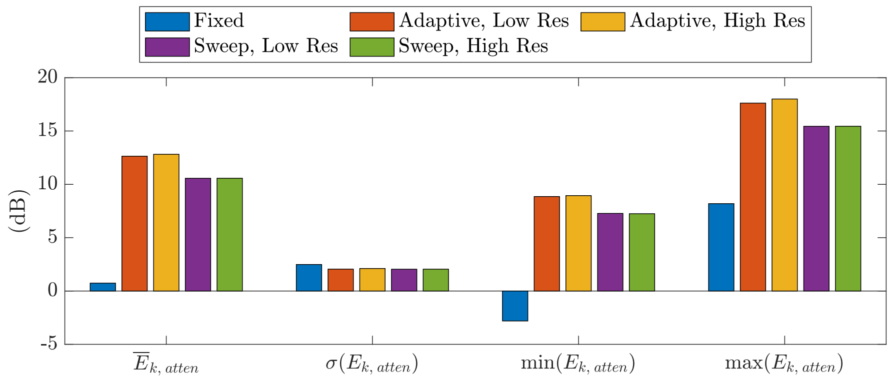

Figure 10: Mean, standard deviation (σ), maximum and minimum attenuation in the kinetic energy with structural uncertainty for the three proposed EDMM tuning approaches.

It can be concluded, based on the results in Figure 10, that out of the investigated tuning approaches in their current configurations, the adaptive system is the most robust to structural uncertainties. Although the high resolution adaptive tuning marginally outperforms the low resolution, this is paid for by a significant increase in the number of shunt circuits required to realise the analogue implementation. Greater robustness in any of the approaches may be achieved by configuring them based on the robust response, rather than only the nominal, but this would require a priori knowledge of the uncertainties and, therefore, an investigation into this is reserved for possible future work. A significant benefit of the adaptive approach is the greatly reduced switching rate considered, which for an analogue circuit is an important consideration. An additional worthwhile consideration in future work would be a comparison between a blind sweep with a sweep rate that results in a comparable switching rate. If the performance of the blind sweep did not deteriorate with the reduction in sweep rate, then the lack of a need for sensors and structural feedback, may make it a more suitable approach in some applications.

6.2. Uncertainties in the Actuator Dynamic Response

In addition to uncertainties in the structural response, it is also relevant to consider the effect of uncertainty in the actuators. Uncertainty in the electrical parameters of the actuators will negate the effect of the shunt and so the shunt design considered here cannot achieve robustness to the electrical parameters and must be modified to address such uncertainty if required. However, it is worth considering the robustness to uncertainty in the mechanical properties of the actuators, as this may highlight potential issues. The effect of uncertainty in the stiffness, mass and damping components of the actuators has therefore been considered. In this case, simulations were run for the nominal structure and the nominal actuator and for 39 additional cases where the three dynamic parameters of the actuators were subject to bounded variation. The variations were set to a linear distribution of ±10 % of the nominal values, which is the range provided in the manufacturer data sheet. The same uncertainty was applied to all of the actuators rather than each having a different response. Although unrealistic, this could be considered the 'worst case' scenario, and may better highlight the difference between the robustness of each tuning approach. The 39 sets of uncertain actuator parameters were chosen in advance using a random number generator and these sets were used for all of the tuning approaches to allow consistent comparisons. Figure 11 shows the amplitude of the mechanical impedance of the resonator to base displacement, Z_r, for the nominal (solid line) and the 39 uncertain models (filled area). Z_r is expressed as

$$Z_r = (\mathrm{j}\omega b_r + k_r)\left(1 - \frac{\mathrm{j}\omega b_r + k_r}{\mathrm{j}\omega b_r + k_r - \omega^2 m_r}\right), \tag{11}$$

where b_r is the actuator damping coefficient, k_r is the actuator suspension stiffness and m_r is the actuator moving mass. From Figure 11 it can be seen how the resonance frequency of the actuator varies with uncertainty, but the variation covers a relatively small range as defined by the bounds of variation set at ±10%.

Figure 12 shows the four previously defined robust performance metrics in the case of uncertainty in the actuator dynamics. It can be seen from these results that all tuning approaches are quite robust to this range of variation in the actuators, with the adaptive and swept approaches both again outperforming the fixed tuning. The adaptive approach again outperforms the swept approach, with the only notable difference to the trend seen in the robustness to structural uncertainty being that the standard deviation in the low resolution adaptive approach is higher than in the swept approach. This could be because, in this case, a change in actuator dynamics shifts the entire sweep bandwidth and, therefore, should maintain a very similar distribution of frequencies around the modal peaks. However, with the adaptive approach, the actuator uncertainty means that the tuning frequencies selected by the algorithm will not be realised accurately and the absorption of the target frequencies will be affected. It can be seen by comparing the other metrics however, that the higher standard deviation for the low resolution adaptive is due to the greater difference between the minimum and maximum values, and the minimum attenuation achieved by the low resolution adaptive is higher than the maximum attenuation achieved by either configuration of the swept approach. The high performance of the adaptive approach is probably aided

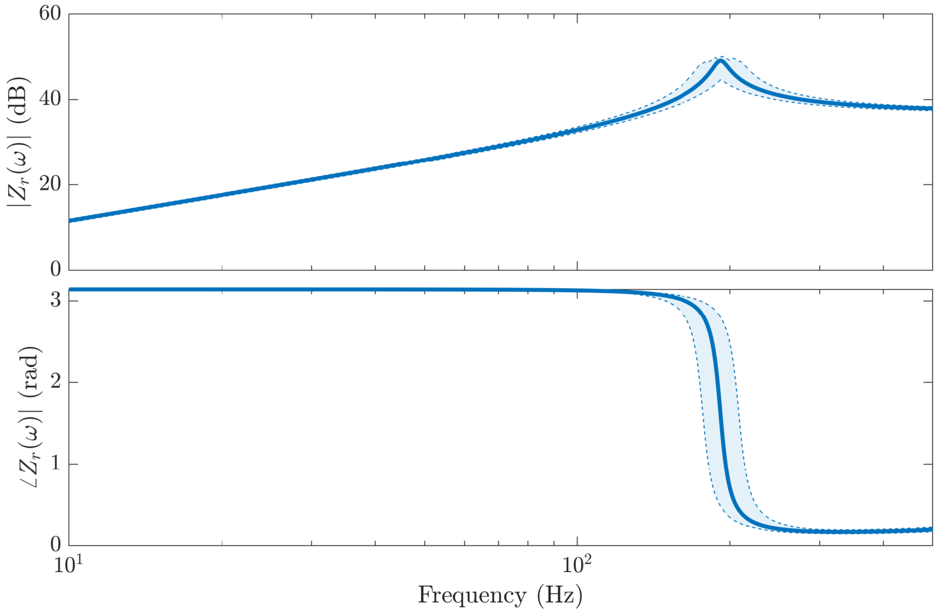

Figure 11: The mechanical impedance of the resonator base to displacement, Z_r, for the nominal case (solid line) and for all cases with uncertainty in the actuator dynamics (filled area).

by the damping of the actuators. Because they are well damped, the mistuning caused by uncertainty is likely to have a reduced effect on the energy of the structure. The difference in robust performance between the swept and adaptive approaches is small, and the discussed benefits of the low switching speed of the adaptive approach still apply. Further investigation is required to understand whether a slower sweep can achieve similar results, and whether configuration of the adaptive approach for an uncertain system has a significant impact on its robust performance. As already stated, all the actuators are assumed to be identical even in the presence of uncertainty. Although this represents a worst case scenario, further investigations should be carried out where this is not the case, with each actuator having a set of uncertain parameters.

7. Conclusions

This paper has presented a variable shunt electrodynamic metamaterial (EDMM) for vibration control, and a novel adaptive tuning approach that provides robustness to uncertainties in the host structure. The EDMM shunt consists of a parallel resistance and inductance or capacitance, allowing the resonance frequency to be tuned up or down in frequency. For a large quantity of differently tuned resonators, it is proposed that an analogue circuit with switching impedances is more practical to implement than individually controlled digital synthetic impedances.

The novel adaptive tuning approach tunes the inertial electrodynamic actuators forming the EDMM unit cell to the centre frequencies of the highest magnitude frequency bins of a short-time Fourier analysis, with logarithmic frequency scale, of the structural velocity. The performance of this tuning approach has been compared to a fixed tuning based on the modal frequencies of a

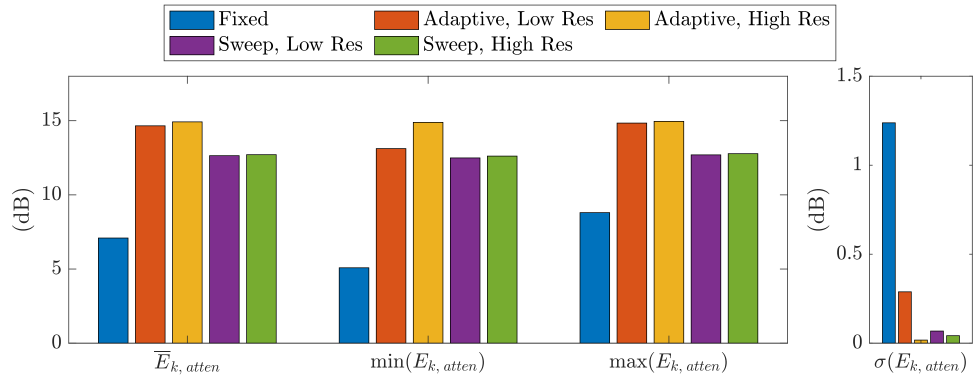

Figure 12: Mean, standard deviation (σ), maximum and minimum attenuation in the kinetic energy with uncertainty in the actuator dynamics for the three proposed EDMM tuning approaches.

nominal host structure, and a discretised "blind sweep" of the tuning frequencies. Investigation into the configuration of the swept approach has demonstrated that the performance on a nominal structure is very robust to the resolution of the discretisation, and to asynchronicity of the sweep across the resonators within the unit cell. However, it is shown that for some configurations, the solver used for the simulations fails to complete. This is due to voltage spikes and instability introduced by switching noise, and future work will look at an apparent relationship between switching rate and the current frequency spectrum. The adaptive tuning approach is shown to outperform the swept approach in attenuating the vibration of a nominal structure. In addition, the switching rate is significantly higher for the swept approach, putting higher strain on any switching matrix components.

In the presence of uncertainties in the modal frequencies of the host structure, the adaptive tuning approach has been shown to achieve greater robustness in all energy metrics. The same result is seen when uncertainties in the mechanical parameters of the inertial actuators forming the EDMM are considered, even though the blind sweep has an advantage in that uncertainty will just shift the sweep range rather than mistuning the individual actuators. This is probably because the actuators are quite damped and therefore the shift in resonance frequency as a result of the uncertainty has a reduced effect.

Acknowledgments

This research was partially supported by an EPRSC iCASE studentship (Voucher number 17100092) and the Intelligent Structures for Low Noise Environments (ISLNE) EPSRC Prosperity Partnership (EP/S03661X/1).

The authors acknowledge the use of the IRIDIS High Performance Computing Facility, and associated support services at the University of Southampton, in the completion of this work.

References

[1] J. Ormondroyd, J. P. Den Hartog, The Theory of the Dynamic Vibration Absorber, Journal of Applied Mechanics 50 (1928) 9–22.

[2] T. Igusa, K. Xu, Vibration Control Using Multiple Tuned Mass Dampers, Journal of Sound and Vibration 175 (4) (1994) 491–503. doi:10.1006/JSVI.1994.1341.
URL `https://www.sciencedirect.com/science/article/pii/S0022460X84713411`
[3] D. P. Hong, Y. S. Ryu, Automatically Controlled Dynamic Absorber (dec 1988).
[4] P. L. Walsh, J. S. Lamancusa, A variable stiffness vibration absorber for minimization of transient vibrations, Journal of Sound and Vibration 158 (2) (1992) 195–211. doi:10.1016/0022-460X(92)90045-Y.
[5] Y. S. Wu, C. C. Lan, Linear variable-stiffness mechanisms based on preloaded curved beams, Journal of Mechanical Design, Transactions of the ASME 136 (12). doi:10.1115/1.4028705.
[6] M. Christie, S. Sun, L. Deng, D. Ning, H. Du, S. Zhang, W. Li, A variable resonance magnetorheological-fluid-based pendulum tuned mass damper for seismic vibration suppression, Mechanical Systems and Signal Processing 116 (2019) 530–544. doi:10.1016/J.YMSSP.2018.07.007.
URL `https://www.sciencedirect.com/science/article/pii/S0888327018304084`
[7] C. Hirunyapruk, M. J. Brennan, B. R. Mace, W. H. Li, A tunable magneto-rheological fluid-filled beam-like vibration absorber, Smart Materials and Structures 19 (5) (2010) 055020. doi:10.1088/0964-1726/19/5/055020.
[8] J. M. Ginder, M. E. Nichols, L. D. Elie, S. M. Clark, Controllable-stiffness components based on magnetorheological elastomers, in: N. M. Wereley (Ed.), Smart Structures and Materials 2000: Smart Structures and Integrated Systems, Vol. 3985, SPIE, 2000, p. 418. doi:10.1117/12.388844.
URL `http://proceedings.spiedigitallibrary.org/proceeding.aspx?doi=10.1117/12.388844`
[9] H.-x. Deng, X.-l. Gong, L.-h. Wang, Development of an adaptive tuned vibration absorber with magnetorheological elastomer, Smart Materials and Structures 15 (5) (2006) N111–N116. doi:10.1088/0964-1726/15/5/N02.
URL `http://stacks.iop.org/0964-1726/15/i=5/a=N02?key=crossref.ffc20e6f5bbfdeb3803f3b4fb443a735`
[10] E. Rustighi, M. J. Brennan, B. R. Mace, A shape memory alloy adaptive tuned vibration absorber: design and implementation, Smart Materials and Structures 14 (1) (2005) 19. doi:10.1088/0964-1726/14/1/002.
[11] M. Berardengo, A. Cigada, F. Guanziroli, S. Manzoni, Modelling and control of an adaptive tuned mass damper based on shape memory alloys and eddy currents, Journal of Sound and Vibration 349 (2015) 18–38. doi:10.1016/J.JSV.2015.03.036.
URL `https://www.sciencedirect.com/science/article/pii/S0022460X15002758`
[12] J. Onoda, T. Endo, H. Tamaoki, N. Watanabe, Vibration suppression by variable-stiffness members, AIAA Journal 29 (6) (1991) 977–983. doi:10.2514/3.59943.
[13] C. Asckler, G. A. Lesieutre, G. H. Koopmann, C. L. Davis, Inertial piezoceramic actuators for smart structures, in: C. R. Crowe, G. L. Anderson (Eds.), Smart Structures and Materials 1995: Industrial and Commercial Applications of Smart Structures Technologies, Vol. 2447, SPIE, 1995, pp. 14–25. doi:10.1117/12.209333.
URL `http://proceedings.spiedigitallibrary.org/proceeding.aspx?articleid=996355`
[14] P. Bonello, M. J. Brennan, S. J. Elliott, J. F. Vincent, G. Jeronimidis, Designs for an adaptive tuned vibration absorber with variable shape stiffness element, Proceedings of the Royal Society A: Mathematical, Physical and Engineering Sciences 461 (2064) (2005) 3955–3976. doi:10.1098/rspa.2005.1547.
URL `https://royalsocietypublishing.org/doi/10.1098/rspa.2005.1547`
[15] C. L. Davis, G. A. Lesieutre, J. J. Dosch, Tunable electrically shunted piezoceramic vibration absorber, in: L. P. Davis (Ed.), Smart Structures and Materials 1997: Passive Damping and Isolation, Vol. 3045, SPIE, 1997, pp. 51–59. doi:10.1117/12.274188.
URL `http://proceedings.spiedigitallibrary.org/proceeding.aspx?articleid=922975`
[16] C. L. Davis, G. A. Lesieutre, Actively tuned solid-state vibration absorber using capacitive shunting of piezoelectric stiffness, Journal of Sound and Vibration 232 (3) (2000) 601–617. doi:10.1006/jsvi.1999.2755.
[17] L. Airoldi, M. Ruzzene, Design of tunable acoustic metamaterials through periodic arrays of resonant shunted piezos, New Journal of Physics 13.
URL `https://iopscience.iop.org/article/10.1088/1367-2630/13/11/113010`
[18] B. S. Beck, K. A. Cunefare, M. Ruzzene, M. Collet, Experimental Analysis of a Cantilever Beam with a Shunted Piezoelectric Periodic Array, Journal of Intelligent Material Systems and Structures 22 (11). doi:10.1177/1045389X11411119.
URL `http://jim.sagepub.com`
[19] S. Chen, G. Wang, J. Wen, X. Wen, Wave propagation and attenuation in plates with periodic arrays of shunted piezo-patches, Journal of Sound and Vibration 332 (6) (2013) 1520–1532. doi:10.1016/j.jsv.2012.11.005.
[20] S. Behrens, A. J. Fleming, S. O. Reza Moheimani, Electromagnetic shunt damping, in: IEEE/ASME International Conference on Advanced Intelligent Mechatronics, AIM, Vol. 2, Institute of Electrical and Electronics Engineers Inc., 2003, pp. 1145–1150. doi:10.1109/AIM.2003.1225504.
[21] C. K. Paulitsch, P. Gardonio, S. J. Elliott, Active vibration damping using a self-sensing electrodynamic actuator, in: K.-W. Wang (Ed.), Smart Structures and Materials 2004: Damping and Isolation, Vol. 5386, SPIE, 2004, p. 282. doi:10.1117/12.539737.
URL `http://proceedings.spiedigitallibrary.org/proceeding.aspx?doi=10.1117/12.539737`

[22] X. Zhang, H. Niu, B. Yan, A novel multimode negative inductance negative resistance shunted electromagnetic damping and its application on a cantilever plate, Journal of Sound and Vibration 331 (10) (2012) 2257–2271. doi:10.1016/j.jsv.2011.12.028.

[23] A. J. McDaid, B. R. Mace, A self-tuning electromagnetic vibration absorber with adaptive shunt electronics, Smart Materials and Structures 22 (10) (2013) 105013. doi:10.1088/0964-1726/22/10/105013.
URL http://stacks.iop.org/0964-1726/22/i=10/a=105013?key=crossref.0dd9001c430d29f821c32faccda5d731

[24] E. Turco, P. Gardonio, Sweeping shunted electro-magnetic tuneable vibration absorber: Design and implementation, Journal of Sound and Vibrationdoi:10.1016/j.jsv.2017.06.035.

[25] E. Turco, P. Gardonio, R. Petrella, L. Dal Bo, Modular vibration control unit formed by an electromagnetic proof-mass transducer and sweeping RL-shunt, Journal of Vibration and Acoustics 142 (6) (2020) 1–35. doi:10.1115/1.4047068.

[26] A. J. Fleming, S. Behrens, S. O. Moheimani, Synthetic impedance for implementation of piezoelectric shunt-damping circuits, Electronics Letters 36 (18) (2000) 1525–1526. doi:10.1049/el:20001083.

[27] J. Nečásek, J. Václavík, P. Marton, Digital synthetic impedance for application in vibration damping, Review of Scientific Instruments 87 (2) (2016) 024704. doi:10.1063/1.4942085.
URL http://aip.scitation.org/doi/10.1063/1.4942085

[28] S. Dalela, P. S. Balaji, D. P. Jena, A review on application of mechanical metamaterials for vibration control, Mechanics of Advanced Materials and Structures (2021) 1–26doi:10.1080/15376494.2021.1892244.
URL https://www.tandfonline.com/action/journalInformation?journalCode=umcm20

[29] G. W. Milton, J. R. Willis, On modifications of Newton's second law and linear continuum elastodynamics, Proceedings of the Royal Society A: Mathematical, Physical and Engineering Sciences 463 (2079) (2007) 855–880. doi:10.1098/rspa.2006.1795.
URL https://royalsocietypublishing.org/doi/10.1098/rspa.2006.1795

[30] H. Sun, X. Du, P. F. Pai, Theory of Metamaterial Beams for Broadband Vibration Absorption, Journal of Intelligent Material Systems and Structures 21 (11) (2010) 1085–1101. doi:10.1177/1045389X10375637.
URL http://journals.sagepub.com/doi/10.1177/1045389X10375637

[31] P. F. Pai, Metamaterial-based Broadband Elastic Wave Absorber, Journal of Intelligent Material Systems and Structures 21 (5) (2010) 517–528. doi:10.1177/1045389X09359436.
URL http://journals.sagepub.com/doi/10.1177/1045389X09359436

[32] H. Peng, P. Frank Pai, Acoustic metamaterial plates for elastic wave absorption and structural vibration suppression, International Journal of Mechanical Sciences 89 (2014) 350–361. doi:10.1016/J.IJMECSCI.2014.09.018.
URL https://www.sciencedirect.com/science/article/pii/S002074031400321X

[33] C. K. Paulitsch, P. Gardonio, S. J. Elliott, Active Vibration Damping Using an Inertial, Electrodynamic Actuator, in: Journal of Vibration and Acoustics, Vol. 129, 2004, p. 39-47. doi:10.1115/1.2349537.
URL http://asmedigitalcollection.asme.org/vibrationacoustics/article-pdf/129/1/39/5736324/39_1.pdf

[34] W. Niu, C. Zou, B. Li, W. Wang Adaptive vibration suppression of time-varying structures with enhanced FxLMS algorithm, in: Mechanical Systems and Signal Processing, Vol. 118, 2019, p. 93-107. doi:10.1016/J.YMSSP.2018.08.009.
URL https://www.sciencedirect.com/science/article/pii/S0888327018304758?via%3Dihub#s0040

[35] L. Singleton, J. Cheer, S. Daley, A robust optimised shunted electrodynamic metamaterial for multi-mode vibration control, Journal of Sound and Vibration 527. doi:10.1016/J.JSV.2022.116861.

[36] S. Miani, M. Zilletti, P. Gardonio, F. Blanchini, P. Colaneri, Switching and sweeping vibration absorbers: Theory and experimental validation, Automatica 93 (2018) 290–301. doi:10.1016/J.AUTOMATICA.2018.03.021.
URL https://www.sciencedirect.com/science/article/pii/S0005109818301080

[37] L. Dal Bo, P. Gardonio, D. Casagrande, S. Saggini, Smart panel with sweeping and switching piezoelectric patch vibration absorbers: Experimental results, Mechanical Systems and Signal Processing 120 (2019) 308–325. doi:10.1016/J.YMSSP.2018.10.024.
URL https://www.sciencedirect.com/science/article/pii/S0888327018306927

[38] J. R. Dormand, P. J. Prince, A family of embedded Runge-Kutta formulae, Journal of Computational and Applied Mathematics 6 (1) (1980) 19–26. doi:10.1016/0771-050X(80)90013-3.

[39] M. E. Hosea, L. F. Shampine, Analysis and implementation of TR-BDF2, Applied Numerical Mathematics 20 (1-2) (1996) 21–37. doi:10.1016/0168-9274(95)00115-8.